

# Control approach of a connected PV system under grid faults

Nejib Hamrouni<sup>1,2</sup> · Moncef Jraidi<sup>1</sup> · Amel Ghobber<sup>1</sup> · Ahmed Dhouib<sup>1</sup>

Received: 12 January 2016 / Accepted: 5 May 2017 / Published online: 13 June 2017  
© Springer-Verlag Berlin Heidelberg 2017

**Abstract** This paper proposes a flexible power control of a three-phase grid-connected PV system which fulfills the PV converter operations under normal conditions and symmetrical grid voltage sags. This control approach can be configured in the PV converters and flexibly change from one to another mode during operation. In normal operation mode, a Maximal Power Point Tracking (MPPT) algorithm and PQ-control loop have been designed around the converters. Their aim is to maximize the PV power and to inject into the grid a current with low harmonic distortion, as well as energy at unity power factor. Under grid voltage dips, the PQ-control strategy has been changed within the grid voltage sag levels and the inverter rating currents. The MPPT control is deactivated, and the PV power has been reduced to the target value delivered by the inverter at the Point of Common Coupling. Case studies with simulations and experimental results have verified the effectiveness and flexibilities of the proposed power control strategy to release the advanced features.

**Keywords** MPPT · Current controller · Grid faults · PQ-control · Grid-connected PV system · Flexible control

## 1 Introduction

The fast expansion of the photovoltaic generators (PVG) in the grid raises voltage deviations such as voltage amplitude drop, frequency deviation and higher harmonic components.

The impact of those problems cannot be ignored on the low voltage-level grid because they affect the availability and the reliability of the distributed grid. The main problems of the grid-connected PV systems are the voltage drops which are characterized by the magnitude: the duration and the phase angle jump [1]. The common cause of these faults is principally the short circuits and the start of the large loads.

Some international regulation codes address that PVG should disconnect from the grid in the presence of voltage drops at the PCC [2]. The Germany standard DIN/VDE 0126 specifies that overvoltage higher than 15% and under-voltage lower than 20% must lead to the disconnection of the PVG within 200 ms. In [3–7], it is required that the PVG ceases to energize local loads in the presence of voltage sags and frequency variations. The disconnection of PVG units, with large scale, from the utility network at the first time of the fault is not an optimal approach. Moreover, the repeated disconnections might have a negative impact on components life time and disturbance of the grid. Hence, it is expected for the future PV converters to have much control flexibility by providing intelligent services. Those functionalities constitute an advantageous solution to further reduce the total cost of PV energy and thus an expansion of cost-effective PV systems into the grid [8,9]. In that case, it is important for the PV systems to provide dynamic grid support in terms of low-voltage ride through (LVRT) [10], in order to stabilize the grid and to avoid loss of a great amount of PV power. Thus, the inverters should stay connected to the grid within a short time and injected some reactive power to support the

---

✉ Nejib Hamrouni  
nejib.hamrouni@inrap.nrnt.tn;  
hamrouni\_nejib2003@yahoo.fr

<sup>1</sup> Laboratory of Analysis and Treatment of Energetic and Electric Systems (ATEES), Science Faculty of Tunis-University of Tunis El Manar, Tunis, Tunisia

<sup>2</sup> High Institute of Science and Technology of Mateur, University of Carthage, Tunis, Tunisia

grid when it presents a voltage dips. As examples, in the German grid code, the PVG should stay connected to the grid when the voltage drops to 0 V in 0.15 s. However, in Italy, any generation systems with power exceeding 6 kW should have LVRT capability [11].

To maintain a stable connection as long as possible of a three-phase grid-connected PV system, under grid disturbances, many control strategies are developed in the literature. They are principally unity power factor control, positive sequence control, constant active power control and constant reactive power control [12–18]. Those works used many power converter topologies for PV systems such as two-stage [19,20] or single-stage [20,21], and with transformer or transformerless [22]. However, the majorities of these papers discussed only the inverter control and omitted the study of the MPPT algorithm.

This paper proposes a flexible power control approach of a three-phase grid-connected PV system which fulfills the PV converter operations under normal conditions and grid voltage sags. In normal operation mode, a MPPT algorithm and PQ-control loop have been designed around the converters in order to maximize the PV power and to provide an ac current with low harmonic distortions. Under grid faults, the proposed control strategy calculates dynamically the active and reactive powers that the inverter can deliver at the PCC. Those values are used as references to calculate the reference currents and to deactivate the MPPT command according to the voltage dips and the inverter rating current. This command is made in dq-rotating reference frame using Proportional-Integral (PI) current controllers, and finally, it is compared to other strategies through experimental results provided by the literature.

This paper is divided into three sections. Section 2 describes the overall system configuration and control structure. Section 3 presents the simulation results and discussions. In the last section, some experimental results have been used to prove the effectiveness of the control strategy.

## 2 Structure and control

Figure 1 shows a generic diagram of a typical double-stage grid-connected PV system. It is composed of a PV array, a dc–dc converter, a voltage source inverter, a LCL-filter to connect the inverter to the grid and a control system. The first stage is adopted to boost up the PV voltage within an acceptable range of the PV inverter [5,7,9] and to set the point of PVG operation in such a way to maximize its power generation. The aim of the second stage is to convert the dc power supplied from the PVG into ac power. A LCL-filter is used to limit the high-order harmonics coming from the inverter switching behavior. The monitoring and control unit consists of voltage sag detection, a power calculation unit,

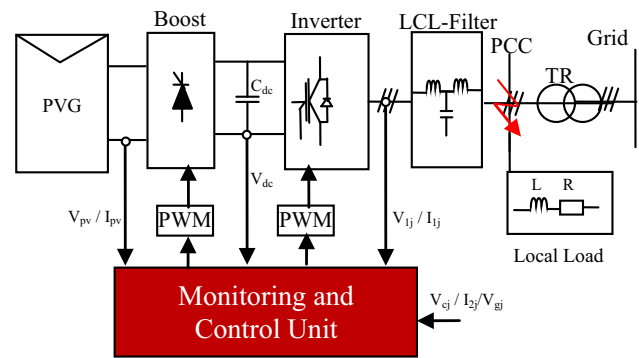


Fig. 1 Diagram of the grid-connected PV system

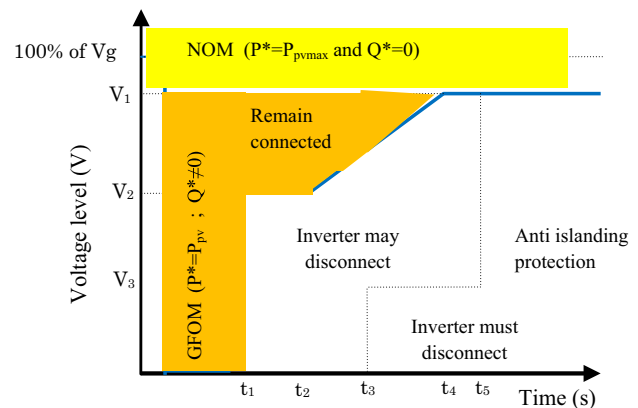


Fig. 2 Low voltage ride through of PV power systems [10]

a current and voltage controllers and a MPPT control. The PV system control is designed considering only the balance voltage dips.

The high penetration of the PVG into the grid raises some requirements, such as the power quality, the frequency and the voltage stability [14]. Moreover, the PVG should stay connected to the grid within a short time and the inverter should inject some reactive power when the grid presents voltage sags. In that case, the control strategy should be developed in order to remain the behavior of the inverter, to stabilize the grid-connected PV system and to avoid the loss of a great PV power generation.

In this paper, a new command scheme for a typical double-stage grid-connected PV system based on PI regulators is proposed. It allowed the grid-connected PV system operation under normal conditions and balance grid voltage sags. In normal operation mode (NOM), the reference active power ( $P^*$ ) is approximately equal to the maximum PV power ( $P^* \approx P_{pvmax}$ ) and the reference reactive power ( $Q^*$ ) is equal to zero.

The control system should switch from the NOM to the grid faulty operation mode (GFOM) once voltage sag was detected [15–18,23]. As indicated by Fig. 2, the inverter

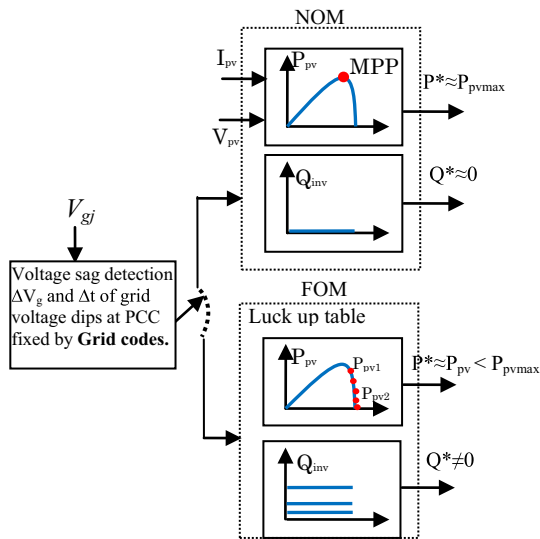
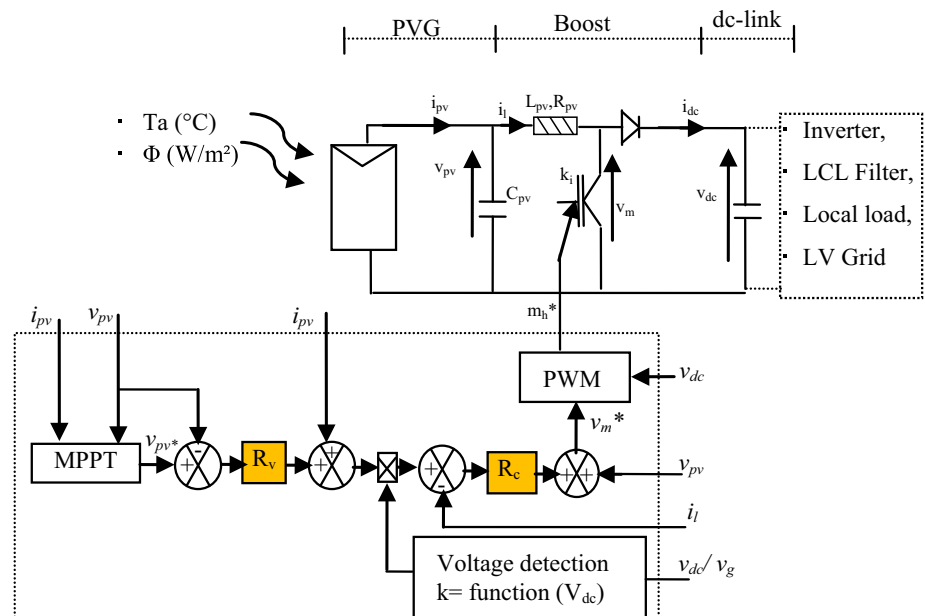


**Fig. 3** Power profiles for a grid-connected PV system in various operation modes

should inject the reactive power according to the grid voltage level and duration [24,25]. The reactive power injected into the grid varied with the voltage sag level, the inverter rating current and the requirements given in [24]. At the same time, the PVG should switch to the non-MPPT functioning mode in order to avoid tripping the inverter over-current protection [26,27]. Therefore, to maintain the stability of the overall system, the power supplied by the PVG should be equal approximately to the inverter output active power. Figure 3 presents the power profiles for the grid-connected PV system in normal and faulty operation modes.

**Fig. 4** Control diagram of the dc–dc converter in various operation modes



### 2.1 Boost control

In NOM, the MPPT algorithm based on Perturbation and Observation (P&O) is employed along with the PVG. The P&O-MPPT algorithm should find the adequate reference voltage ( $V_{pv}^*$ ) imposed by the dc–dc converter to the system. The reference voltage ( $V_{pv}^*$ ), given by the MPPT algorithm, constitutes the input of the voltage and the current controllers. As indicated by Fig. 4, voltage and current control loops are used in cascade with the MPPT algorithm allowing the control of the PV energy stored in the output filter ( $L_{pv}C_{pv}$ ). The voltage control loop with the PV current compensations provides the reference current ( $I_1^*$ ), while the current control loop with the PV voltage compensations give the reference voltage ( $V_m^*$ ) for PWM. The boost converter command signal is given, according to [28], by:

$$m_h^* = \frac{v_m^*}{v_{dc}} \tag{1}$$

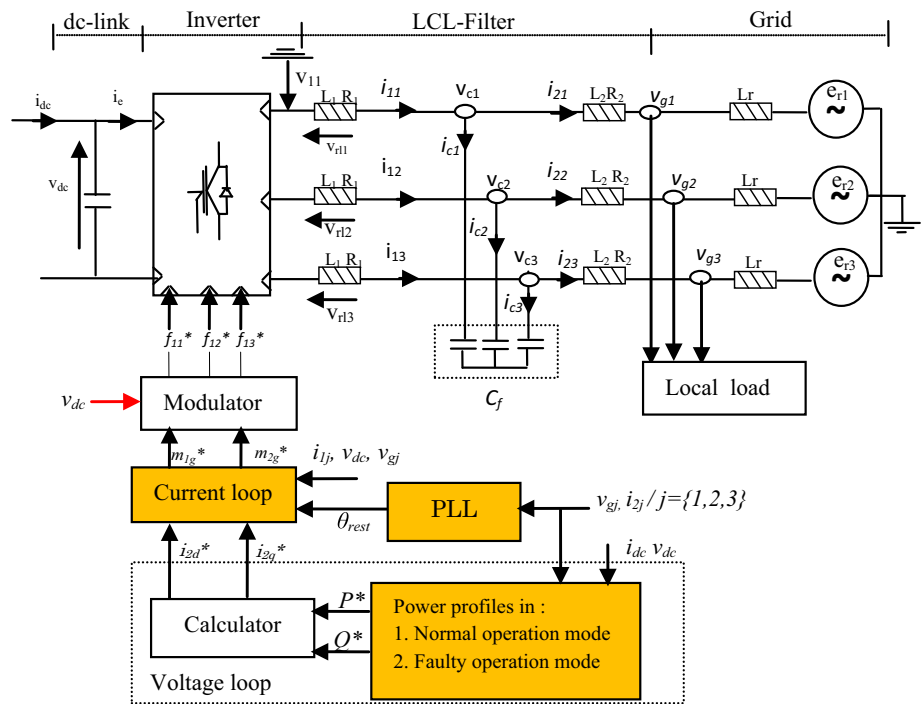
where

$$v_m^* = R_c R_v v_{pv}^* + (1 - R_c R_v) v_{pv} + R_{ci_{pv}} - R_c i_l \tag{2}$$

$R_c$  and  $R_v$  represent, respectively, the PV current and the voltage regulators. When the boost switch frequency is higher, the time constant is very small and its influence to the whole system may be ignored, so proportional correctors are sufficient. They are parameterized according to the value of the capacitor ( $C_{pv}$ ), the inductance ( $L_{pv}$ ) and the dynamic of the regulation loops [29].

Under grid sags, the inverter output current should increase to keep the power constant [30]. The output current

**Fig. 5** Block diagram of the inverter command



is limited by the inverter maximum rating current ( $I < I_{max}$ ) which avoids inverter to shut down. In this case, the inverter output power became lower than the dc power delivered by the PVG. Thus, the difference is stored in the dc-link capacitor. As a consequence, the dc-link voltage increases and exceeds its limit ( $V_{max}$ ) which makes the PV system disconnected from the grid network. In that case, to limit the dc-link voltage, it should limit the power delivered by the PVG. As a solution, the PV panel should switch to the non-MPPT operation mode in order to avoid tripping the inverter over-current protection. Practically, this method is based on the multiplication of the reference PV current by a coefficient varying between 0 and 1 according to the level of the grid sags. Consequently, the PV current injected by the PVG decreased and then the MPPT is deactivated. The coefficient is selected as follows:

- If  $V_{dc} < V_{max}$ , then  $k = 1$ .
- If  $V_{dc} > V_{max}$ , then  $k = f(V_{dc})$  and varies between 0 and 1.

**2.2 Inverter control**

The main goal of the inverter control, in normal operation mode, is to transfer all PV power produced into the grid, to regulate the dc-link voltage and to set a unity power factor for the grid currents. The proposed control scheme is two loops based as indicated in Fig. 5. The outer loop is the dc-link voltage, and the inner one is around the inverter output currents. Three elementary command blocks around

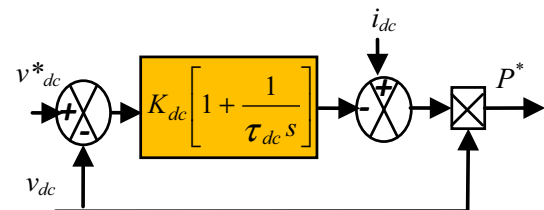


**Fig. 6** Diagram of the dc-link voltage controller

the inverter appear: the dc-link voltage controller, the current loop and the phase-locked loop (PLL). Under grid sags, the inverter control should switch to the GFOM. The reactive and active power references should be changed within the voltage sag level and the inverter rating current. The proposed control scheme of the inverter in NOM and GFOM is given by Fig 5.

The power control configured in the PV converters can change from one to another mode according to the state of the grid voltage at the PCC. This approach based on the PQ theory permits the possibilities to generate appropriate reference currents for the current controller (Figs. 6, 7).

**2.2.1 Voltage loop**

The voltage loop is composed of two modules which ensure the control of the dc-link voltage and the calculation of the reference currents. In normal operation mode, the first module supplies a dc current allowing the calculation of the active

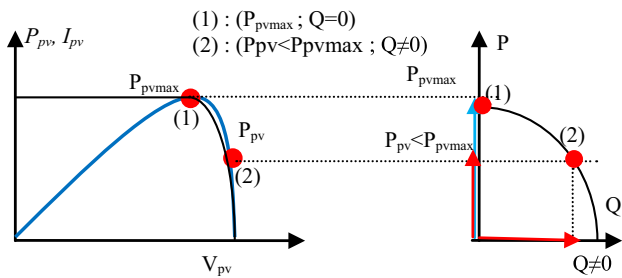


**Fig. 7** PQ diagram and photovoltaic PV curve; 1 NOM, 2 GFOM

power reference injected into the grid. It is given by:

$$P^* = V_{dc} \cdot i_c^* \approx P_{pv \max} \tag{3}$$

whereas the reference reactive power ( $Q^*$ ) should be zero in order to obtain the line current in phase with the grid voltage. The objective of the voltage control loop is to regulate the dc-link voltage at a specified value and to provide the reference current. The closed-loop control of the dc-link voltage is needed because the output power of the PVG varied with irradiance and temperature. The inverter input reference current  $i_c^*$  is described by the following relation [28]:

$$i_c^* = i_{dc} - PI(v_{dc}^* - v_{dc}) \tag{4}$$

To control the dc-link voltage, a Proportional-Integral (PI) corrector has been used. It is parameterized according to the capacitor and the dynamic of the regulation loop [31]. The dc-link voltage reference ( $v_{dc}^*$ ) is set to 515 V.

Under grid sags, the required active and reactive power references should be changed. According to [7], they are given by:

$$\begin{cases} P^* = \frac{3}{2} V_g I_{2d} \approx P_{pv} \\ Q^* = \frac{3}{2} V_g I_{2q} \neq 0 \end{cases} \tag{5}$$

where  $V_g$  is the amplitude value of the grid voltage and  $P_{pv}$  is the output power provided by the PVG when the boost command switches to the non-MPPT control. The required active power was lower than the maximum PV power delivered in the normal conditions ( $P^* < P_{pv \max}$ ). According to [32], the inverter should change its output power within the level of the voltage sags. The reference power ( $P^*$ ) is around the maximal PV power ( $P_{pv \max}$ ), if the voltage dip is small, contrary, if the voltage dip is equal to zero,  $P^*$  should be equal to zero.

The second module of the voltage loop is devoted to the calculation of the reference currents  $i_{2d}^*$  and  $i_{2q}^*$  which are used in the current loops. Reference currents  $i_{2d}^*$  and  $i_{2q}^*$  are calculated from the grid voltage and the reference active and reactive power references. These currents, according to [33],

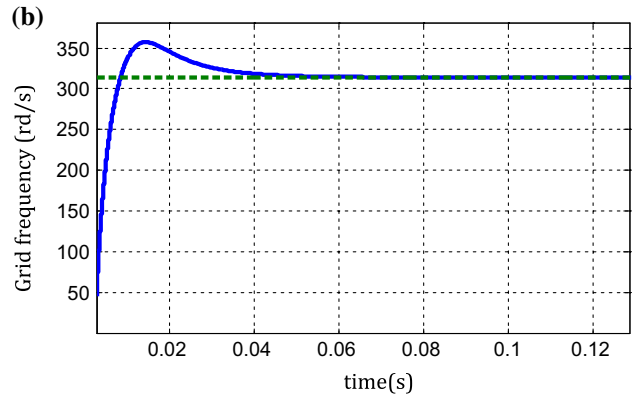
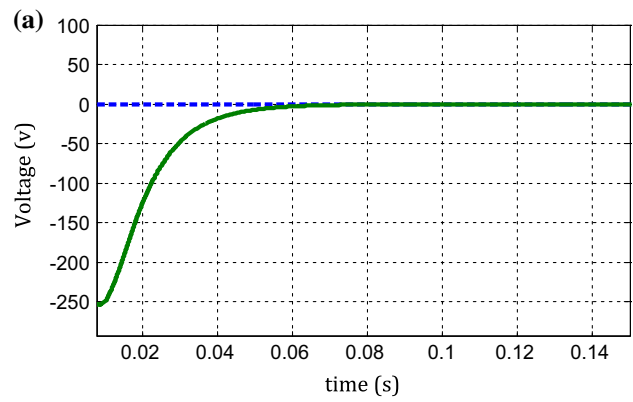


**Fig. 8** Behavior of the proposed PLL in NOM: **a** grid voltage  $q$  and  $d$ -components (measure and reference), **b** grid frequency estimation

are expressed in the synchronous reference dq-frame by:

$$\begin{bmatrix} i_{2d}^* \\ i_{2q}^* \end{bmatrix} = \frac{1}{V_{gq}^2 + V_{gd}^2} \begin{bmatrix} P^* & -Q^* \\ Q^* & P^* \end{bmatrix} \begin{bmatrix} V_{gd} \\ V_{gq} \end{bmatrix} \tag{6}$$

### 2.2.2 PLL loop

According to Eq. 6, the reference currents injected into the grid are deduced from the measure of the grid voltages. Indeed, the network voltages at the PCC can contain various faults (voltage dips, harmonics, short interruptions, etc.) which can pass into the current provided by the inverter. To mitigate this problem, several methods are developed in the literature [34].

Among those methods, we are interested in PLL expressed in dq-frame. This method is able to provide the grid frequency and phase information. The grid phase provided by the PLL will be used in the current loop unit. The PLL regulator should be designed to respond within a minimum of overshoot under grid frequency and voltage variations. According to Fig. 8, when the difference between grid phase angle ( $\theta_{rest}$ ) and inverter angle ( $\theta_{ond}$ ) is reduced to zero, the PLL became active and we obtain:  $v_{gd} = 0$  and  $v_{gq} = -\sqrt{3}V_r$ [34]. The model of the PLL is strongly non-linear. However, to synthe-



size the PLL corrector, we considered a linearized model for weak variations of grid phase angle ( $\theta_r$ ) as given by Fig. 9. To avoid oscillation of the PLL response, the damping factor should be equal to 1, and then, it permits consequently the deducing of the various regulator parameters.

### 2.2.3 Current loop

The ac current controller is considered particularly suitable for active inverters for its safety and stability performance. It consists of a model-based cascade controller. It is composed of an outer current controller for the network line current, i.e., current  $i_{2j}$ , an intermediate voltage controller for the filter capacitor voltage and an inner current control loop for the inverter current  $i_{1j}$ , where  $j = \{1, 2 \text{ and } 3\}$

According to Fig. 5, the current loop should drive the output current  $i_{2d}$  and  $i_{2q}$  to the desired steady-state current, namely to the shape and phase of the utility grid voltage by generating control signals  $m_1^*$  and  $m_2^*$  for PWM. The line current is implemented in the synchronously rotating reference dq-frame. Hence, individual controllers for the active and reactive quantities with additional compensation for the cross coupling of the d and q axis components are obtained. This current controller block is common for both NOM and FGOM. Its inputs are the d and q current components generated by the voltage loop ( $i_{2d}^*$  and  $i_{2q}^*$ ). According to the state space description of the output LCL-filter model [29], the reference voltages are given by:

$$\begin{cases} v_{cd}^* = L_2 \frac{d}{dt} (i_{2d}^*) + R_2 i_{2d} - \omega_{rest} L_2 i_{2q} + v_{gd} \\ v_{cq}^* = L_2 \frac{d}{dt} (i_{2q}^*) + R_2 i_{2q} + \omega_{rest} L_2 i_{2d} + v_{gq} \end{cases} \quad (7)$$

The voltage  $v_{cdq}^*$  is composed of two terms: the first represents the network voltage ( $v_{gdq}$ ) which is directly measured, whereas the second represents the voltage drop of the equivalent impedance when it is crossed by the current  $i_{2dq}$ .

The inverter output reference currents are given by:

$$\begin{cases} i_{1d}^* = C_f \frac{dv_{cd}^*}{dt} - C_f \omega_{rest} v_{cq} + i_{2d} \\ i_{1q}^* = C_f \frac{dv_{cq}^*}{dt} - C_f \omega_{rest} v_{cd} + i_{2q} \end{cases} \quad (8)$$

In (8), the reference current is composed of two terms. The first term represents the network current ( $i_{2dq}$ ) which is directly measured, whereas the second represents the current crossed the capacitor when it is feed by the voltage  $v_{cdq}$ .

The reference voltages, in the inverter-side, are given by:

$$\begin{cases} v_{1d}^* = L_1 \frac{d}{dt} (i_{1d}^*) + R_1 i_{1d} - \omega_{rest} L_1 i_{1q} + v_{cd} \\ v_{1q}^* = L_1 \frac{d}{dt} (i_{1q}^*) + R_1 i_{1q} - \omega_{rest} L_1 i_{1d} + v_{cq} \end{cases} \quad (9)$$

The first term in (9) represents the capacitor voltage  $v_{cdq}$  which is directly measured, whereas the second term rep-

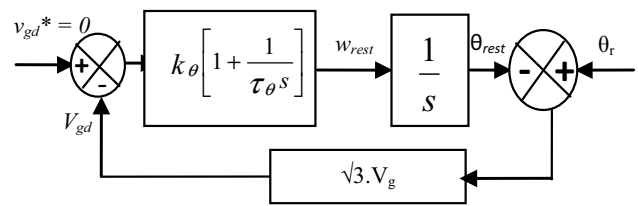


Fig. 9 Structure of linearized PLL model

resents the voltage drop of the filter impedance when it is crossed by a current  $i_{1dq}$ .

According to [35], terms 7, 8 and 9 should be elaborated by the control loops. The control structure consists of three cascade regulators with additional feed forward and feed-back terms given by the LCL-filter model. In order to stabilize the system, the gains of the proportional parts are altered from the deadbeat gain by the constants  $k_{i1}$ ,  $k_{uc}$  and  $k_{i2}$ . Their values are obtained from the stability analysis given in [36] (Fig. 9).

## 3 Simulations

### 3.1 Normal operation mode

Under normal grid conditions, the grid-connected PV system is operating in Maximum Power Point Tracking mode, in order to deliver as much energy as possible to the grid network and to obtain a power factor near the one. The most important waveforms simulated are shown in Figs. 10, 11. These simulations have been obtained under constant irradiance ( $1000 \text{ W/m}^2$ ) and temperature ( $25^\circ\text{C}$ ). They are selected to demonstrate the most significant aspects of the system behavior. The reference and the measure are represented by dotted and continuous line, respectively. Salient parameters of the system and regulators are presented in Tables 1, 2. The PV generator is a polycrystalline 24 V/45Wc-AEGPQ40D.

Figure 10 shows the characteristics of the active and reactive powers provided during the normal grid conditions ( $1000 \text{ W/m}^2$ ,  $25^\circ\text{C}$ ). This figure presents the maximum PV power supplied by the PV panels, reactive and active powers injected into the grid, respectively. At steady state, real power through the inverter is controlled and reactive power is forcefully made zero. The reactive power oscillates around its reference ( $Q^* = 0 \text{ VAR}$ ) showing unity power factor operation and control performance of the grid current. The measured active power supplied by the inverter oscillates around its maximum reference ( $P \approx P_{pvmax}$ ).

It can be seen that, in normal operation mode, the inverter output power follows its reference and that average power control has been established. The power injected by the PV panel is approximately equal to the inverter output power because the converter losses are neglected. Accord-

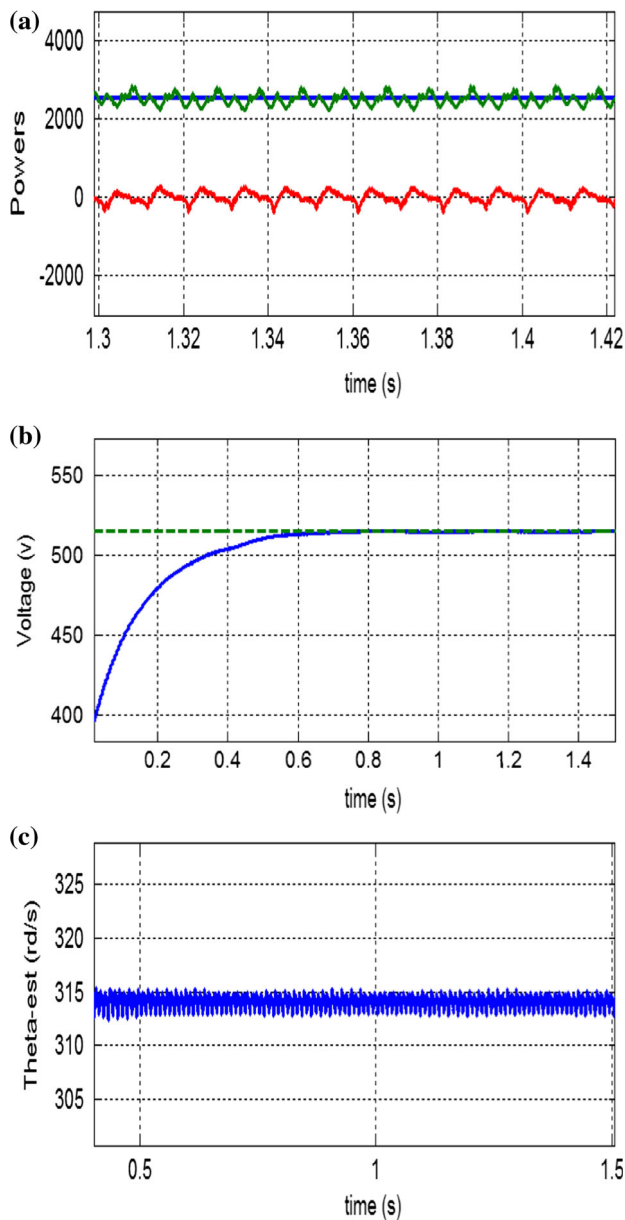


**Fig. 10** Simulation results under constant climatic conditions: **a** Maximum PV power (blue), inverter output active (green) and reactive (red) powers, **b** dc-link voltage (reference and measure), **c** grid phase provided by the PLL (color figure online)

ing to Fig. 10b, the dc-link voltage, maintained at a constant level, followed instantaneously its deadbeat reference voltage ( $V_{dc}^*$ ). Consequently, the active power extracted from the PVG is completely injected into the grid. Figure 10c presents the grid phase estimated by the PLL. It oscillates around its nominal value equal to 314rd/s.

In the inverter side, the measured current and voltage d-components as depicted in Fig. 11 followed their references. They show the higher performances of the various control loops designed around the PV converters.

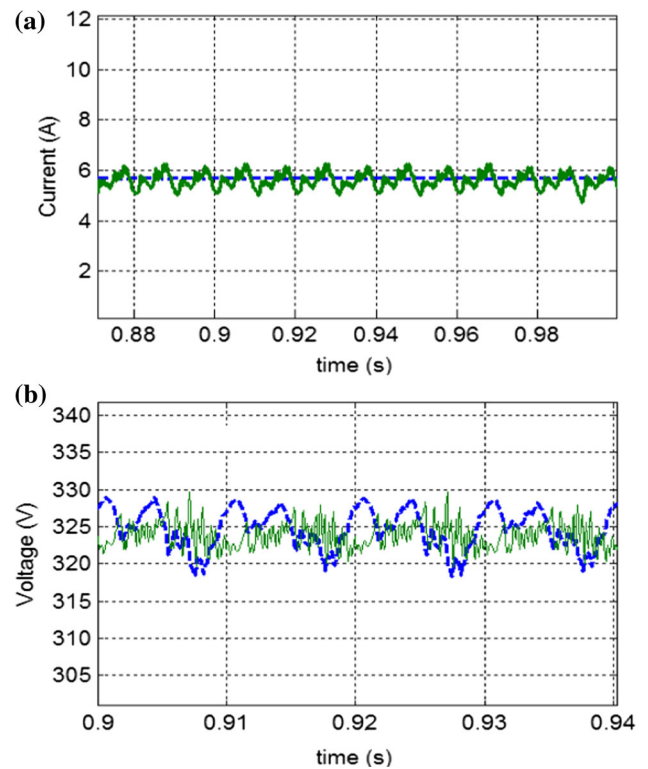


**Fig. 11** Simulation results (measure and reference) under constant climatic conditions: **a** Inverter current d-components, **b** inverter voltage d-components

### 3.2 Grid faulty operation mode

In this section, attention is devoted to the grid fault influence and contribution in a grid-connected PV system. In order to study and to analysis the behavior of the proposed strategy and the control scheme in a grid faulty operation mode, a balance three-phase grid voltage sag is applied at the PCC. The following figures illustrated the response of the grid-connected PV system under a balance grid dip characterized by magnitude and duration (110 V–100 ms).

#### 3.2.1 Enabled of the MPPT command

In the PV converter side, output current, voltage and active power of the PVG are also as the same because the MPPT control stay enabled. As indicated by Fig. 12, the PV current and voltage remain nearly their references. The error between the reference and the measured PV current has been caused by the approximation made during the design of the PV current controller. The voltage dip has not an influence on the maximum power provided by the dc–dc converter because the dc-link capacitor acts as a buffer zone. As shown by Fig. 13, when the transient fault occurs, the active and reactive powers deviate from their nominal values. The real power decreases to 1.6 kW while the reactive power rises up to 280 VAR in

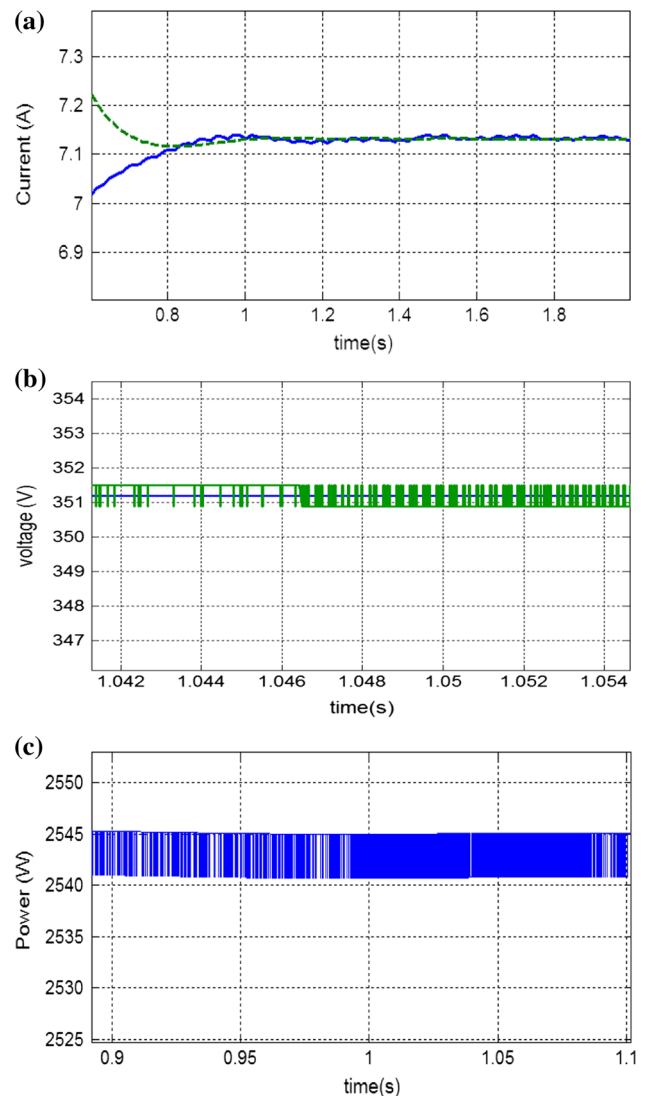
**Table 1** Principal parameters of the system

Parameter	value
Cell series resistance $R_s$	0.011 $\Omega$
Cell parallel resistance $R_p$	10.35 $\Omega$
Ideal constant of diode $n$	1.25
Cell reverse saturation current $I_s$	$13.89 \cdot 10^3 T^3 \exp(-13.2 \cdot 10^3 / T)$ A
Photocurrent of PVG $I_{ph}$	$[2.807 + 1.4 \cdot 10^{-3} (T - T_{ref})] \varnothing$ A
Cell reference temperature $T_{ref}$	298.15 °K
Series cell $n_s$	40
Parallel cell $n_p$	1
Series modules $N_s$	20
Parallel modules $N_p$	3
Short-circuit current of PVG $I_{sc}$	8.37 A
Open-circuit voltage of PVG $V_{pv0}$	428 V
Output PV filter resistance $R_{pv}$	1 $\Omega$
Output PV filter capacitance $C_{pv}$	0.005 °F
DC-link Capacitance $C_{dc}$	0.009 °F
Filter inductance $L_1$	19 mH
Filter resistance $R_1$	0.5 $\Omega$
Filter capacitance $C_f$	10 $\mu$ F
Filter inductance $L_2$	20 mH
Filter resistance $R_2$	0.5 $\Omega$
Grid inductance $L_r$	0.005 H
Grid resistance $R_r$	1 $\Omega$
Maximal PV current $I_{pvmax}$	7.2 A
Maximal PV voltage $V_{pvmax}$	340 VA

**Table 2** Principal parameters of the PI regulators

Parameter	value
Gain of PV voltage regulator $R_v$	10
Gain of PV current regulator $R_c$	34
Gain of dc-link voltage regulator $k_{dc}$	0.001
Const. time of dc-link voltage regulator $\tau_{dc}$	0.1
Gain of PLL regulator $K_\theta$	10
Constant time of PLL regulator $\tau_\theta$	0.1
Gain of the inverter output current regulator $ki_1$	50
Const. time of the inverter output current regulator $\tau_{i1}$	0.002
Gain of the voltage regulator $kv_c$	0.05
Const. time of the voltage regulator $\tau_{v_c}$	0.002
Gain of the filter output current regulator $ki_2$	10
Const. time of the filter output current regulator $\tau_{i2}$	0.003

order to withstand the voltage dip. The PV power oscillates around the Maximal Power Point (MPP) because the P&O-MPPT algorithm is enabled. When the voltage decreased

**Fig. 12** Simulation results (measure and reference) under grid sags: **a** PV current, **b** PV voltage, **c** maximum PV power

to 50%, the inverter output current increases and becomes equal to the saturation output inverter current. Then the output inverter power becomes lower than the PV power injected by the PV panel. The difference between the PV power and the inverter output power ( $P_{pvmax} - P_{inv}$ ) is accumulated in the dc-link capacitor. As a consequence, the dc-link voltage ( $V_{dc}$ ) increases to a high level (650 V) which can destroy the capacitor. Normally, the protection system should disconnect the inverter from the grid because the dc-link voltage exceeds the internal protection. Figure 13a shows that, after the suppressed of faults, the inverter output power ( $P_{inv}$ ) decreases slightly and reaches the maximum PV power ( $P_{pvmax}$ ) in 200 ms. As indicated by Fig. 13b, the dc-link voltage decreases progressively discharging the energy into the grid and reaches its reference in 200 ms. The voltage d-component of the LCL-filter, as depicted in Fig. 13c, follows its refer-



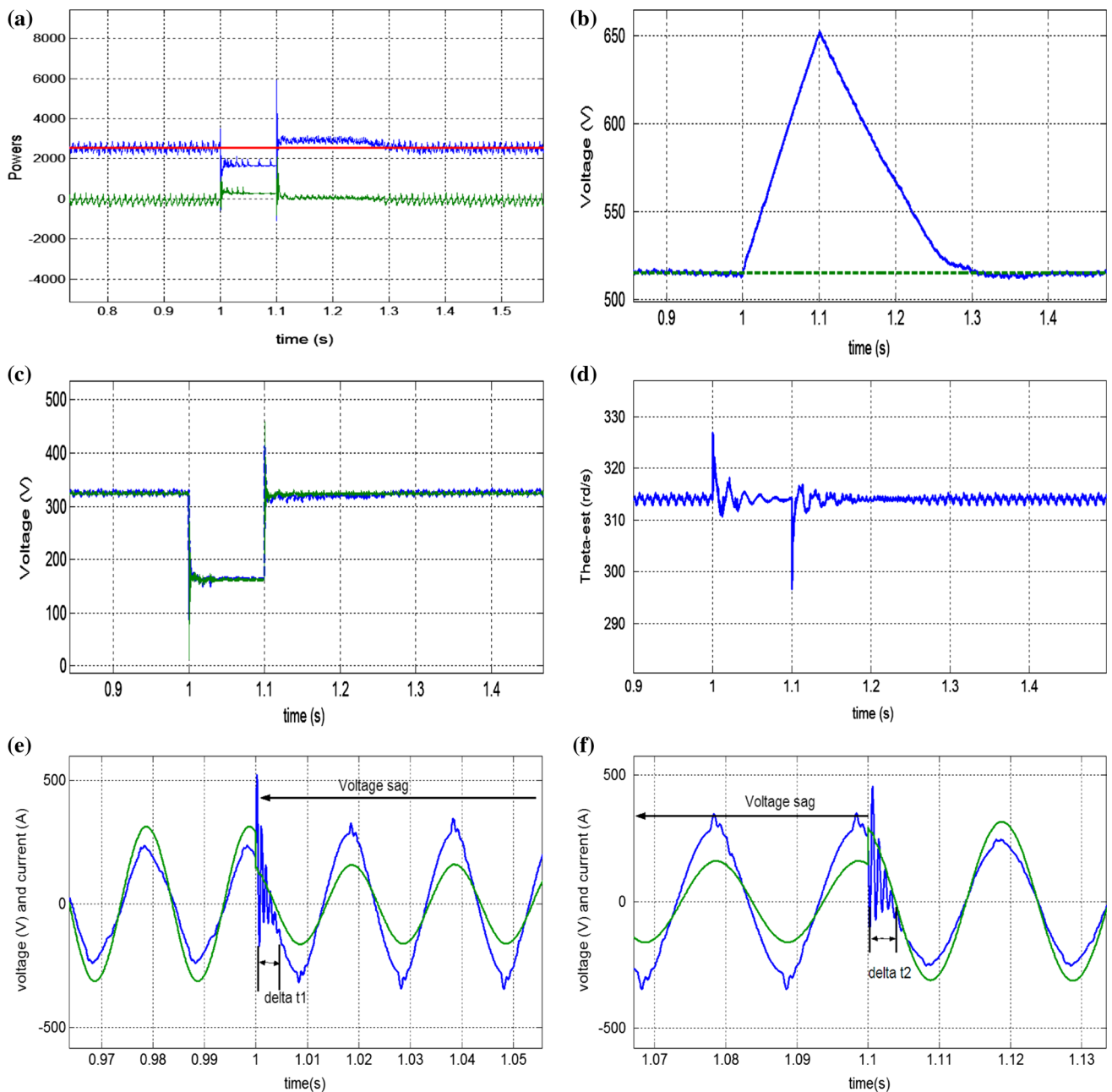


**Fig. 13** Simulation results under grid sags: **a** maximum PV power (red), inverter output active (blue) and reactive (green) powers, **b** dc-link voltage (measure and reference), **c** inverter voltage *d*-component

(measure and reference), **d** grid frequency provided by the PLL, **e, f** grid voltage (green) and ( $\cdot 40$ ) inverter output current (blue) (color figure online)

ence provided by the controller. It shows the performances of the controller in GFOM.

Figure 13d illustrates the grid frequency estimated by the PLL. It presents some overshoot at the time of grid voltage drops. As it can be seen in this figure, the performances of the PLL are poor during the voltage sag. It was clear that the PLL dynamics present a significant role in transient behavior of the grid-connected PV system. Figure 13e, f shows the ac side

voltage and the inverter output current at the PCC. As it might be noticed in those figures, there is a phase leading/lagging between grid side line current and voltage. A low displacement can be noticed between the synthesized current, current effectively injected into the grid, and the line voltage. As a result, the unit power factor is not achieved under grid voltage dips. For instance, the inverter should provide a reactive power. Both the start of the voltage dip and the end of that

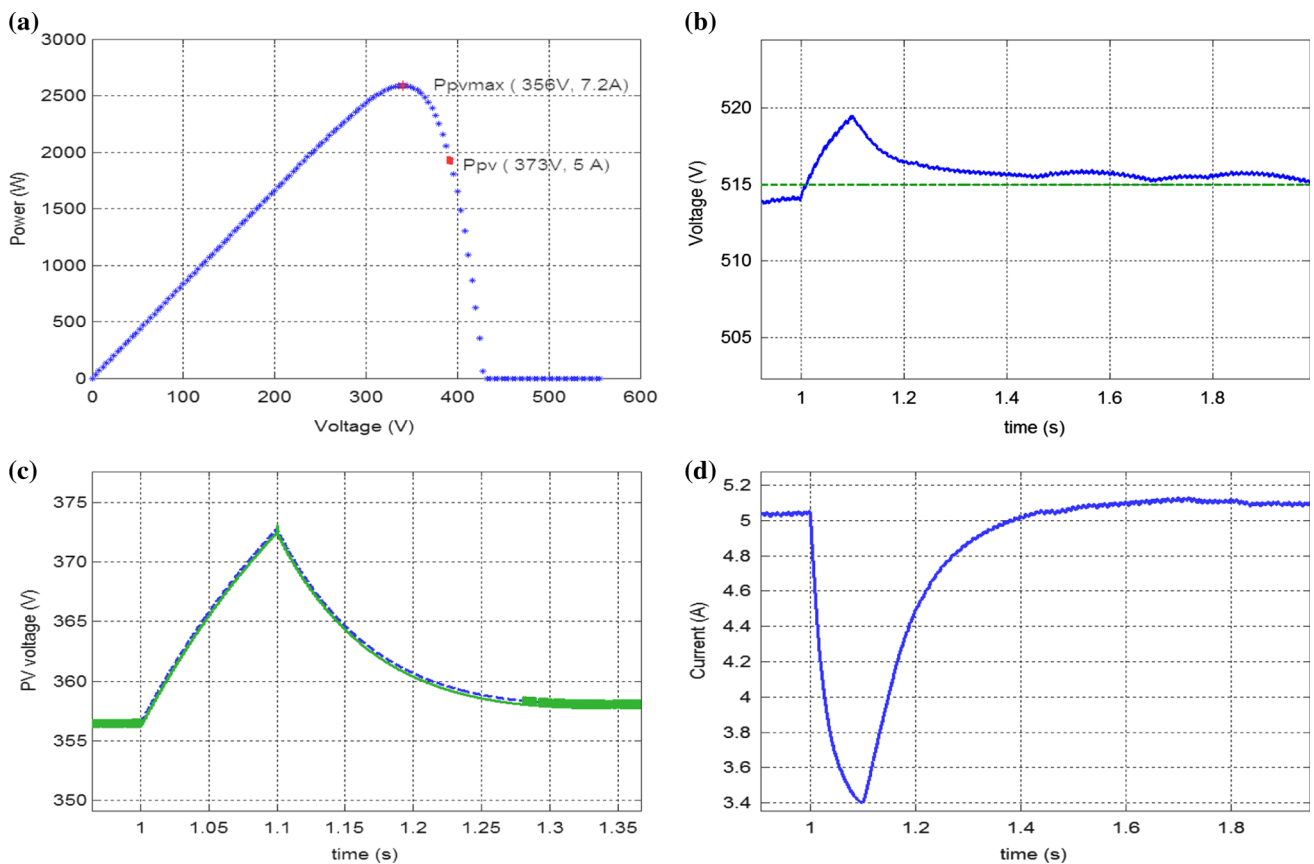


**Fig. 14** Simulation results under grid sag: **a** PV operation point on P–V curve in various operation modes, **b** dc-link voltage (reference and measure), **c** PV voltage (reference and measure), **d** dc current injected by the dc–dc converter

present a transient current oscillations, respectively,  $\Delta i_{t1}$  and  $\Delta i_{t2}$ . The current waveform is rather distorted due to the synchronizing problem. The control succeeds to resynchronize the inverter very quickly after voltage recovery.

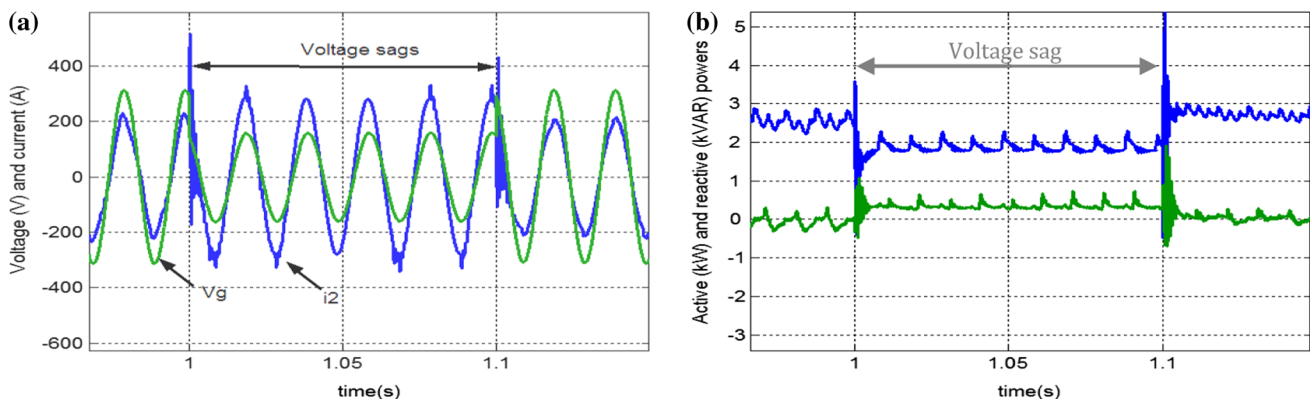
### 3.2.2 Disabled of the MPPT command

According to Fig. 14a, the maximum PV power ( $P_{pvmax}$ ) is 2563 W, and the PV voltage ( $V_{pvmax}$ ) and the PV current ( $I_{pvmax}$ ) at the maximum power are 356 V and 7.2 A, respectively. Once the grid sag is detected at 1 s, the MPPT is deactivated and the control system is switched to the grid faulty operation mode. The PVG provides a new power which is lower than the optimal PV power. In the same time, the inverter starts to inject reactive power to support the grid voltage and limits the active power output to prevent the inverter from over current protection. The active power provided by the PVG decreases in order to maintain the dc-link voltage lower than the limit value (Fig. 14b). Moreover, the PV voltage increases to 373 V by respecting the PV characteristics (Fig. 14c). Figure 14d shows the characteristic of the dc current provided by the boost during the various operation modes. In normal operation mode, the continuous current is

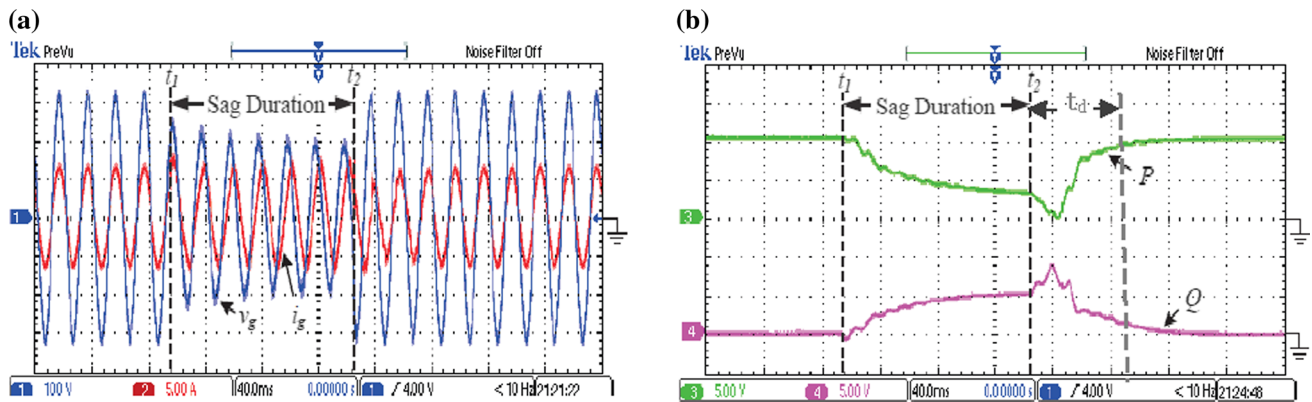
equal to 5 A. The power provided by the PVG was maximal, and it was equal approximately to 2550 W. When the control system switched to the fault operation mode, the current decreased until 3.4 A. After 100 ms, the fault is cleared and the grid-connected PV system goes back to its normal operation mode. In the same time, the MPPT unit continues to track the optimal PV power. As shown in Fig. 14b, d, the system takes some time to join its normal state because of the MPPT process.

Figure 15 illustrates the response of the grid-connected PV system to 50%–00 ms voltage dip which can occur on the grid voltage at the PCC. Figure 15b presents the inverter output active and reactive power variations. It is shown that during the fault, the PV system is controlled to limit the active power ( $\approx 1900$  W) and to inject some reactive power ( $\approx 280$  VAR) into the grid. As illustrated by Fig. 14a, the PV inverter increases the ac current when the grid voltage decreases to keep the power constant. During the step transient in the grid voltage, there is a phase leading/lagging between grid side line current and voltage.

Figures 14, 15 illustrate the performances and dynamics of the command approach when the MPPT algorithm is disabled. This command permits to the inverter to support the



**Fig. 15** Simulation results under grid sags: **a** grid voltage and ( $\cdot$ 40) current, **b** inverter output active (blue) and reactive (green) powers (color figure online)



**Fig. 16** Experimental results of a single-phase system under voltage dip: **a** grid voltage and inverter current, **b** real and reactive powers

grid within a short time when it presents a voltage dips. This example of study shows that when the grid voltage dips stay lower than the thresholds fixed in [37], the command approach allows the system operations with the injection of reactive power and the reduce of the active power.

### 4 Experimental results

For the verification of the proposed approach, we refer to some experimental results studies in [38]. The whole system consists mainly of:

- A dc power supply the nominal dc-link voltage.
- A dc capacitor (1100  $\mu$ F),
- A Danfoss VLT FC302 3-phase inverter which is configured as a single-phase inverter. Its rated current is equal to 5A.
- A sag generator,
- An LCL<sub>t</sub>-filter connects the inverter to the grid ( $L = 1.8$  mH,  $C = 4.3$   $\mu$ F and  $L_t = 4$  mH).
- A FPGA control system.

For the laboratory test, the nominal grid voltage is set to 220 V RMS, the frequency is equal to 50 Hz and the PWM frequency is set to 8 kHz. The control strategy has been tested under voltage sag (50%–100 ms).

Figure 16 shows the performance of the inverter under grid voltage dip with the flexible power control strategy. It shows that the control is able to operate even during a very shallow voltage dip. As it can be seen before the grid fault, the reactive power is zero and the real power supplied by the inverter is constant and maximal. An inverter current THD, lower than 5%, around the rated inverter output current, has been achieved (Fig. 16a). When a grid voltage occurs, the control system reduces the output active power ( $P$ ) and increases slightly the reactive power ( $Q$ ) according to the depth of the voltage sag in order to withstand the dip (Fig. 16b). The end of the fault presents a transient time delay ( $t_d$ ) due to the fault detection and the response of the controllers. The inverter can stay connected and energizes the grid in the presence of voltage sags.

Figure 17 shows a zoom on the waveforms (current and voltage) obtained when the grid voltage is subjected to a (50%–100 ms) voltage dip. During the fault, the inverter tends

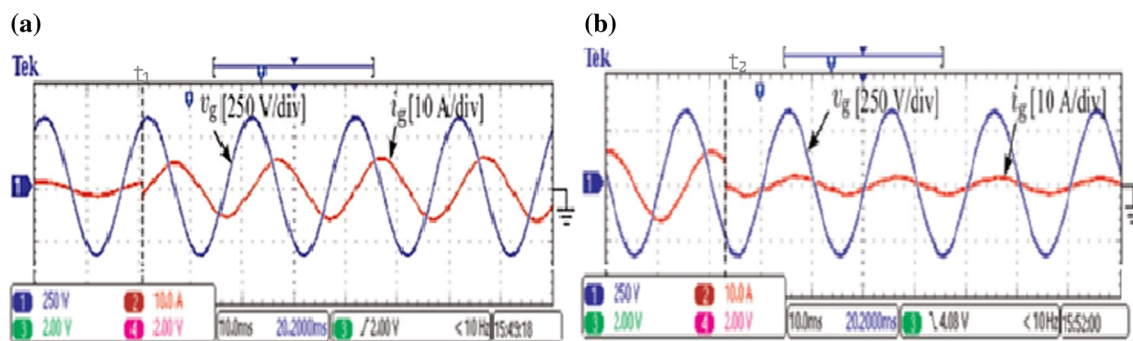


**Fig. 17** Experimental results of a single-phase system under voltage dip: **a**, textbf grid voltage and inverter current

to increase the ac current when the voltage decreases at PCC. At the same time, a phase leading/lagging between grid side line current and voltage appears. In that case, a reactive current is injected into the grid in response to the grid faults.

According to Fig. 16, it has been observed that the current control loop is very fast and able to respond to voltage disturbances in two cycles. This behavior is very positive since it would tend to mitigate voltage dips. The flexible power control succeeds to resynchronize the inverter very quickly after voltage recovery. When the voltage sag is cleared, the system returns to its normal operation mode and injects current at unity power factor.

Referring to Figs. 15, 16, it is seen that the experimental results are in agreement with the simulation results shown in Figs. 14, 12e, f, and have corroborated the effectiveness and the flexibility of the proposed control strategy.

The theoretical results can be very helpful for the study of the transient properties of the inverter (decoupling protection, current control loop and MPPT tracker, etc.) and allow PV converters to have a better tolerance to shallow voltage dips without threatening the safety and stability of the connected PV system. Hence, the flexible power control strategy, proposed in this study, can be an enhancement for the future PV converters. It contributes to reduce the cost of energy and thus enables more cost-effective PV installations.

## 5 Conclusion

In this paper, a control strategy approach has been developed around a double-stage grid-connected PV system functioning under various operation modes. It is observed that, during the NOM, the command ensures a maximum PV power and regulates simultaneously the dc-link voltage and the output inverter currents. Moreover, it permits to inject energy into the grid at unity power factor and a current with low harmonic distortion. In the GFOM, the active and reactive power references have been changed within the voltage sag levels and the inverter rating current. The inverter delivered a reactive

power slightly greater than zero and decreased the output active power in order to stabilize the whole system. In the GFOM, we demonstrate that the control strategy ensures a grid sinusoidal current at the PCC and provides ride through capability during grid faults. Moreover, this command contributes to the system stability and overcomes some problems such as harmonic distortions and power factor quality. It has been demonstrated that the proposed control strategy improves the availability and the reliability of the distributed network under grid faults. Hence, it is expected for the future PV converters to have some ancillary and intelligent service like flexible active power control and reactive power compensation. Together with higher efficiency and higher demands, those functionalities represent the key to reduce the total cost of energy and thus an expansion of cost-effective PV systems into the grid.

## References

1. Milanovic JV, Djokic SZ (2003) Equipment sensitivity to disturbances in voltage supply. In: JIEEC, Bilbao
2. Teodorescu R, Liserre M, Rodriguez P (2011) Grid converters for photovoltaic and wind power systems. Wiley, London
3. Yang Y, Wang H, Blaabjerg F (2014) Reactive power injection strategies for single phase photovoltaic systems considering grid requirements. In: 29 Annual IEEE-APECE, pp 371–378
4. Yang Y, Blaabjerg F, Zou Z (2013) Benchmarking of grid fault modes in single-phase grid-connected photovoltaic systems. IEEE Trans Ind Appl 49(5):2167–2176
5. Cadaval ER, Spagnuolo G, Franquelo LG, Paja CAR, Suntio T, Xiao WM (2013) Grid-connected photovoltaic generation plants: components and operation. IEEE Ind Electron Mag 7(3):6–20
6. Yang Y, Enjeti P, Blaabjerg F, Wang H (2013) Suggested grid code modifications to ensure wide-scale adoption of photovoltaic energy in distributed power generation systems. In: IEEE-IAS annual meeting, pp 1–8
7. Carnieletto R, Brandao DI, Farret FA, Simoes MG (2011) Smart grid initiative: a multifunctional single-phase voltage source inverter. IEEE Ind Appl Mag 17(5):27–35
8. Yeh HG, Gayme DF, Low SH (2012) Adaptive VAR control for distribution circuits with photovoltaic generators. IEEE Trans Power Syst 27(3):1656–1663



9. SMA Profitable Night Shift, Technical Information (2013). [www.sma.de](http://www.sma.de)
10. Iov F, Hansen AD, Sorensen PE, Cutululis NA (2007) Mapping of grid faults and grid codes. Riso National Laboratory, Technical University of Denmark, Roskilde
11. Comitato Elettrotecnico Italiano (2011) Reference technical rules for connecting users to the active and passive LV distribution companies of electricity. In: CEI 0–21
12. Rodriguez P, Luna A, Munoz-Aguilar R, Corcoles F, Teodorescu R, Blaabjerg F (2011) Control of power converters in distributed generation applications under grid fault conditions. In: ECCE, pp 2649–2656
13. Azevedo MGS, Rodriguez P, Cavalcanti MC, Vázquez G, Neves FAS (2009) New control strategy to allow the photovoltaic systems operation under grid faults. In: COBEP, Brazilian, pp 196–201
14. Yang Y, Blaabjerg F (2013) Low voltage ride through capability of a single phase photovoltaic system connected to the low voltage grid. *Int J Photo Energy* 2013:9
15. Kai D, Cheng KWE, Xue XD (2006) A novel detection method for voltage sags. In: ICPESA, pp 250–255
16. Lee DM, Habetler TG, Harley RG, Keister TL, Rostron JR (2007) A voltage sag supporter utilizing a PWM-switched auto transformer. *IEEE Trans Power Electron* 22(2):626–635
17. Bae B, Lee J, Jeong J, Han B (2010) Line-interactive single phase dynamic voltage restorer with novel sag detection algorithm. *IEEE Trans Power Deliv* 4(25):2702–2709
18. Fitzer C, Barnes M, Green P (2004) Voltage sag detection technique for a dynamic voltage restorer. *IEEE Trans Ind Appl* 1(40):203–212
19. Casaro M, Martins DC (2008) Grid-connected PV system: introduction to behavior matching. In: PESC-IEEE, pp 951–956
20. Kjaer SB, Pedersen JK, Blaabjerg F (2002) Power inverter topologies for photovoltaic modules—a review. In: 37th IAS annual meeting conference, vol 2, pp 782–788
21. Azevedo GMS, Cavalcanti MC, Neves FAS, Rodriguez P (2007) Implementation of a grid connected photovoltaic system controlled by digital signal processor. In: COBEP, Blumenau
22. Kerekes T, Teodorescu R, Klumpner C, Sumner M, Florica D, Rodriguez P (2009) Evaluation of three phase transformerless photovoltaic inverter topologies. *Power Electron* 24(9):2202–2211
23. Hernandez OCM, Enjeti PN (2005) A fast detection algorithm suitable for mitigation of numerous power quality disturbances. *IEEE Trans Ind Appl* 6(41):1684–1690
24. Bae Y, Vu TK, Kim RY (2013) Implemental control strategy for grid stabilization of grid-connected PV system based on German grid code in symmetrical low-to-medium voltage network. *IEEE Trans Energy Convers* 3(28):619–631
25. Arnold G (2011) Challenges of integrating multi-GW solar power into the German distribution grids. <http://www.iwes.fraunhofer.de/>
26. Chou SF, Lee CT, Cheng PT, Blaabjerg F (2011) A reactive current injection technique for renewable energy converters in low voltage ride-through operations. In: IEEE-PES general meeting, pp 1–7
27. Lee CT, Hsu CW, Cheng PT (2011) A low-voltage ride through technique for grid-connected converters of distributed energy resources. *IEEE Trans Ind Appl* 4(47):1821–1832
28. Mogos EF (2004) Production dans les réseaux de distribution, étude pluridisciplinaire de la modélisation pour le contrôle des sources. PHD Thesis, ENSAM, Lille
29. Hamrouni N (2009) Modélisation et commande des systèmes photovoltaïques connectés au réseau électrique basse tension. PHD Thesis, ENIT, Tunisie
30. Mahmoud AMA, Mashaly HM, Kandil SA, El Khaseb H, Nashed MNF (2000) Fuzzy logic implementation for photovoltaic maximum power tracking. In: IEEE international workshop on robot and human interactive communication, pp 155–60
31. Hamrouni N, Jraidi M, Chérif A (2008) New control strategy for 2-stage grid-connected photovoltaic system. *Renew Energy* 33:2212–2222
32. Kobayashi H (2012) Fault ride through requirements and measures of distributed PV systems in Japan. In: IEEE-PES general meeting, pp 1–6
33. Akagi H, Nabae A (1986) Control strategy of active power filters using multiple voltage source PWM converters. *IEEE Trans Indus Electr* 22(3):460–465
34. Pankow Y (2005) Etude de l'intégration de la production décentralisée dans un réseau basse tension, application au générateur photovoltaïque. PHD Thesis, ENSAM, France
35. Alali MAE (2002) Contribution à l'étude des compensateurs actifs des réseaux électriques basse tension. PHD Thesis, University Louis Pasteur, Strasbourg, France
36. Bojrup M (1999) Advanced control of active filters in a battery charger application. PHD Thesis, Lund Institute of Technology
37. Jamali S, Talavat V (2010) Dynamic fault location method for distribution networks with distributed generation. *Electr Eng J* 92:119–127
38. Yang Y, Blaabjerg F, Huai W, Marcelo GS (2016) Power control flexibilities for grid-connected multi-functional photovoltaic inverters. *IET Renew Power Gener* 99:1–10